

Enhanced mass-loss rate evolution of stars with $\gtrsim 18M_{\odot}$ and missing optically-observed type II core-collapse supernovae

RONI ANNA GOFMAN,¹ NAOMI GLUCK,² AND NOAM SOKER^{1,3}

¹*Department of Physics, Technion, Haifa, 3200003, Israel; rongof@campus.technion.ac.il; soker@physics.technion.ac.il*

²*Department of Physics, Stony Brook University, New York, United States; naomi.gluck@stonybrook.edu*

³*Guangdong Technion Israel Institute of Technology, Shantou 515069, Guangdong Province, China*

ABSTRACT

We evolve stellar models with zero age main sequence (ZAMS) mass of $M_{\text{ZAMS}} \gtrsim 18M_{\odot}$ under the assumption that they experience an enhanced mass-loss rate when crossing the instability strip at high luminosities, and conclude that most of them end as type Ibc supernovae (SNe Ibc) or dust-obscured SNe II. We examine the hydrogen mass in the stellar envelope and the optical depth of the dusty wind at explosion, and crudely estimate that only about a fifth of these stars explode as unobscured SNe II and SNe Iib. About 10-15 percent end as obscured SNe II that are infrared-bright but visibly very faint, and the rest, about 65-70 percent end as SNe Ibc. Our findings have implications to the ‘red supergiant problem’, referring to the death of observed core-collapse supernovae with $M_{\text{ZAMS}} \gtrsim 18M_{\odot}$, as we conclude that it is possible that all these stars actually do explode as CCSNe. However, the statistical uncertainties are still too large to decide whether many stars with $M_{\text{ZAMS}} \gtrsim 18M_{\odot}$ do not explode as expected in the neutrino driven explosion mechanism, or whether all of them explode as CCSNe, as expected by the jittering jets explosion mechanism.

Keywords: Supernovae — stars: jets — stars: variables: general — binaries: general

1. INTRODUCTION

The two theoretical mechanisms to power core-collapse supernova (CCSN) explosions from the gravitational energy that the collapsing core releases are: the delayed neutrino mechanism (Bethe & Wilson 1985), and the jittering jets explosion mechanism (Soker 2010; or more generally the jet feedback mechanism, e.g., Soker 2016). Each of these mechanisms in its originally-proposed form encounters some problems that require the addition of some ingredients.

The extra ingredient that recent numerical simulations of the delayed neutrino mechanism introduce to overcome some of the basic problems of the original delayed neutrino mechanism (for these problems see, e.g., Papish et al. 2015; Kushnir 2015), is convection above the iron core in the pre-collapse core (e.g., Couch & Ott 2013, 2015; Mueller & Janka 2015; Müller et al. 2017, 2019). The flow fluctuations of the convective zone that ease explosion results in large-amplitude stochastic angular momentum variations of the mass that the newly born neutron star (NS) accretes. These fluctuations seem to lead to the launching of a bipolar outflow with varying symmetry axis directions, namely, jittering jets (Soker 2019b).

Indeed, the jittering jets explosion mechanism is based on such flow fluctuations in the convective regions of the pre-collapse core or envelope (Gilkis & Soker 2014, 2015; Quataert et al. 2019). The spiral standing accretion shock instability (SASI) and other instabilities behind the stalled shock at about 100 km from the newly born NS amplify these fluctuations (for the physics of the spiral SASI see, e.g., Blondin & Mezzacappa 2007; Iwakami et al. 2014; Kuroda et al. 2014; Fernández 2015; Kazeroni et al. 2017). However, results of numerical simulations that find no stochastic accretion disks around the newly born NS brought to the recognition that neutrino heating plays a role in the jittering jets explosion mechanism (Soker 2018, 2019a). In a recent study, Soker (2019b) analyses three-dimensional hydrodynamical simulations of CCSNe and concludes that both neutrino heating and accretion of stochastic angular momentum operate together to launch jittering jets that explode CCSNe.

One of the places where the delayed neutrino mechanism and the jittering jets explosion mechanism differ from each other is the prediction of the outcome of stars with zero age main sequence (ZAMS) mass of $M_{\text{ZAMS}} \gtrsim 18M_{\odot}$. According to the delayed neutrino mechanism for most of the masses in that range

the core-collapse to form a black hole in a failed supernova, i.e., there is no explosion (e.g., Fryer 1999; Horiuchi et al. 2014; Sukhbold et al. 2016; Ertl et al. 2016; Sukhbold, & Adams 2019; Ertl et al. 2019), but rather only a faint transient event (Lovegrove & Woosley 2013; Nadezhin 1980). According to the jittering jets explosion mechanism, on the contrary, there are no failed CCSNe, and all of these stars do explode, even if the collapsing core forms a black hole. According to the jittering jets explosion mechanism when a black hole is formed the outer core material and then the envelope gas contains enough stochastic angular momentum (e.g., Gilkis & Soker 2014, 2015; Quataert et al. 2019) to launch jets and set an energetic explosion, up to $E_{\text{exp}} > 10^{52}$ erg (Gilkis et al. 2016).

These different predictions of the two explosion mechanisms relate directly to the so-called red supergiant (RSG) problem (Smartt et al. 2009), referring to the finding that the observed relative number of progenitors of CCSNe II with ZAMS masses of $M_{\text{ZAMS}} \gtrsim 18M_{\odot}$ is much lower than their relative number on the main sequence (e.g., Jennings et al. 2014; Williams et al. 2014; for a review see, e.g., Smartt 2015). Smartt (2015) argues in his thorough review of the ‘red supergiant problem’ that it is consistent with the claim of the delayed neutrino mechanism that most stars of $M_{\text{ZAMS}} \gtrsim 18M_{\odot}$ collapse to form black holes with no visible supernovae, but possibly a faint transient event. Adams et al. (2017) suggest that the star N6946-BH1 that erupted in 2009 (Gerke et al. 2015) was a failed SN event of a progenitor of $\approx 25M_{\odot}$. Kashi, & Soker (2017) provide an alternative interpretation to that event based on a transient event (intermediate luminosity optical transient–ILOT) that was obscured by dust in the equatorial plane that happens to be along our line of sight.

We do note that there are claims for massive progenitors of some CCSNe, e.g., a progenitor of the type IIIn SN 2010jl of mass $M_{\text{ZAMS}} \gtrsim 30M_{\odot}$ (Smith et al. 2011), and a possible SN Ic progenitor with a mass of $M_{\text{ZAMS}} \gtrsim 50M_{\odot}$ (Van Dyk et al. 2018).

One possible explanation to the missing massive progenitors of CCSNe II might be an obscuration by dust (e.g., Walmswell, & Eldridge 2012), but one should properly calculate dust extinction in CCSNe (Kochanek et al. 2012).

Jencson et al. (2017) claim that if the two events they studied in the infrared (IR) are CCSNe, then-current optical surveys miss $\gtrsim 18\%$ of nearby CCSNe. In a more systematic study Jencson et al. (2019) find nine IR bright transients, and estimate that 5 of these events are dust-obscured CCSNe. They further estimate that optical surveys miss $\approx 40\%$ (the range of 17 – 64%) of

all CCSNe. If holds, this might cover most (or even all) stars with $M_{\text{ZAMS}} \gtrsim 18M_{\odot}$, implying that these stars also explode as CCSNe.

The recent results of Jencson et al. (2019), that are compatible with the expectation of the jittering jets explosion mechanism, motivate us to reexamine the possibility that stars with $M_{\text{ZAMS}} \gtrsim 18M_{\odot}$ forms a much dense circumstellar matter (CSM) than stars with $M_{\text{ZAMS}} \lesssim 18M_{\odot}$. Yoon, & Cantiello (2010) already studied the process by which partial ionisation of hydrogen in the envelope causes RSG stars to strongly pulsate and lose mass at a very high rate (e.g., Heger et al. 1997). They further discussed the possibility that this enhanced mass-loss rate of stars with $M_{\text{ZAMS}} \gtrsim 19 - 20M_{\odot}$ might explain the RSG problem, by both forming an optically thick dusty CSM and by removing most, or even all, of the hydrogen-rich envelope and forming a SN of type Ib or Ic (Ibc) progenitor. We continue the idea of Yoon, & Cantiello (2010) but perform somewhat different evolutionary simulations. We assume that the stars have enhanced mass-loss when they cross the continuation of the instability strip on the HR diagram when they are RSGs. We strengthen the claim of Yoon, & Cantiello (2010) that such an enhanced mass-loss rate might account for RSG problem, allowing all stars to explode as CCSNe.

In Section 2, we describe our numerical setup, and in Section 3 we present the calculation of evolutionary tracks under the assumption that RSG stars that cross the instability strip have very high mass-loss rates. In Section 4 we study the dust properties that might obscure stars with $18M_{\odot} \lesssim M_{\text{ZAMS}} \lesssim 20M_{\odot}$, and also find that this possibly enhanced mass-loss rate brings more stars of $M_{\text{ZAMS}} \gtrsim 20M_{\odot}$ to explode as types IIb or Ib CCSNe. We summarise our main conclusions in section 5.

2. NUMERICAL SET UP

We evolve stellar models with ZAMS mass in the range of $M_{\text{ZAMS}} = 15 - 30M_{\odot}$ using Modules for Experiments in Stellar Astrophysics (MESA, version 10398 Paxton et al. 2011, 2013, 2015, 2018). Each model has an initial metallicity of $Z = 0.02$, and evolves from the pre-main sequence stage until pre-core-collapse, which we take to be the first time the iron core has an inward velocity ≥ 1000 km.

We employ mixing according to a mixing-length theory (Henyey et al. 1965) with $\alpha_{\text{MLT}} = 1.5$ in convective regions defined by the Ledoux criterion. Semiconvection is used with $\alpha_{\text{sc}} = 1.0$ (Langer et al. 1983). Step function convective overshooting is applied with an overshooting parameter of 0.335 (Brott et al. 2011).

We apply wind mass-loss with the MESA "Dutch" mass-loss scheme for massive stars which combines results from several papers and is based on [Glebbeek et al. \(2009\)](#). For $T_{\text{eff}} > 10^4$ K and surface hydrogen abundance larger than 0.4 the "Dutch" scheme uses [Vink et al. \(2001\)](#) and for surface hydrogen abundance lower than 0.4 it uses [Nugis & Lamers \(2000\)](#). In cases where $T_{\text{eff}} < 10^4$ K mass-loss is treated according to [de Jager et al. \(1988\)](#).

We break up the evolution to two parts: inside the instability strip and outside it. Figure 1 in [Georgy et al. \(2013\)](#) shows the Hertzsprung Russell (HR) diagram for non-rotating models with an instability strip in the range of $2 \lesssim \log(L/L_{\odot}) \lesssim 5$ and $3.5 \lesssim \log(T_{\text{eff}} [\text{K}]) \lesssim 3.8$. From that figure we approximate that the instability strip to be in the region where

$$64 \lesssim \log\left(\frac{L}{L_{\odot}}\right) + 16.4 \log\left(\frac{T_{\text{eff}}}{[\text{K}]}\right) \lesssim 65. \quad (1)$$

We extend the instability strip to higher luminosities. While the star is outside the strip we set the mass-loss scaling factor to $f_{\text{ml}} = 0.8$ since the models have no rotation ([Maeder, & Meynet 2001](#)). When the star crosses the extended part of the instability strip from right to left on the HR diagram, namely at very late evolutionary phases, we consider one of three cases for the mass-loss rate. In the first case, we assume that the instability strip has no special role, and we keep $f_{\text{ml}} = 0.8$. The other 2 cases have enhanced mass-loss inside the instability strip. Once the model enters the strip from right to left we increase the mass-loss scaling factor to $f_{\text{ml}} = 2$ in one case and to $f_{\text{ml}} = 10$ in another. We base our prescription for enhanced mass-loss rate in the instability strip on the results of [Yoon, & Cantiello \(2010\)](#) who argue that RSG stars lose mass at a very high rate when they are inside the instability strip on the HR diagram.

3. RESULTS

In this section, we focus mostly on the effect of the mass-loss rate inside the instability strip on the pre-collapse state of the stellar models. We evolve over 40 stellar models up to the point of core-collapse with 16 different values of ZAMS mass for each of the three mass-loss parameters, f_{ml} , that we set in the instability strip.

Fig. 1 shows the evolution of some models on the HR diagram, while for others we show only the final position. We also present the instability strip, including our extension to high luminosity. It is evident that by increasing the mass-loss rate when the star is inside the instability strip (extension) and crosses from right to left, the pre-collapse effective temperature of models that leave the strip increases.

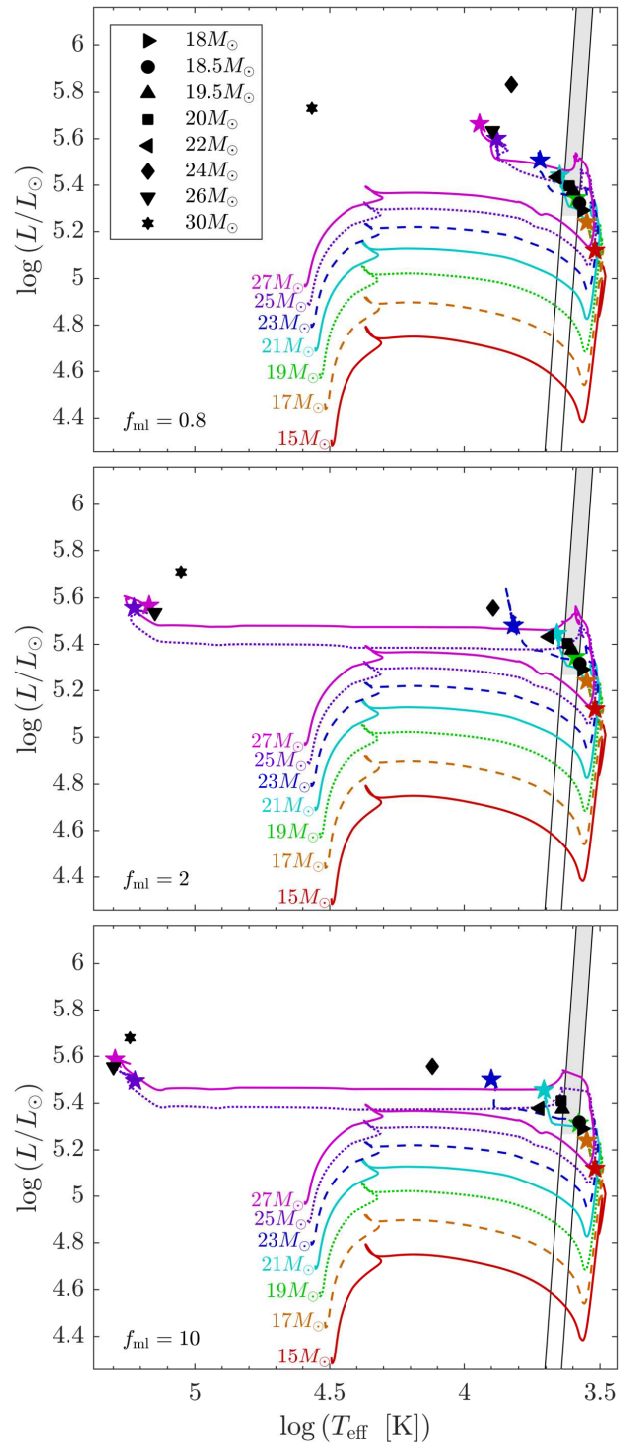


Figure 1. The evolution track of stellar models with ZAMS masses in the range of 15–30 M_{\odot} from ZAMS to core-collapse on the HR diagram. The pre-collapse point of each model is marked by a coloured pentagram for odd masses and a black marker for all other masses. The instability strip and its extension according to equation (1) is marked with two black lines. The panels have different mass-loss scaling factors, f_{ml} as given in the inset when a star crosses the instability strip from right to left in the grey area of the strip.

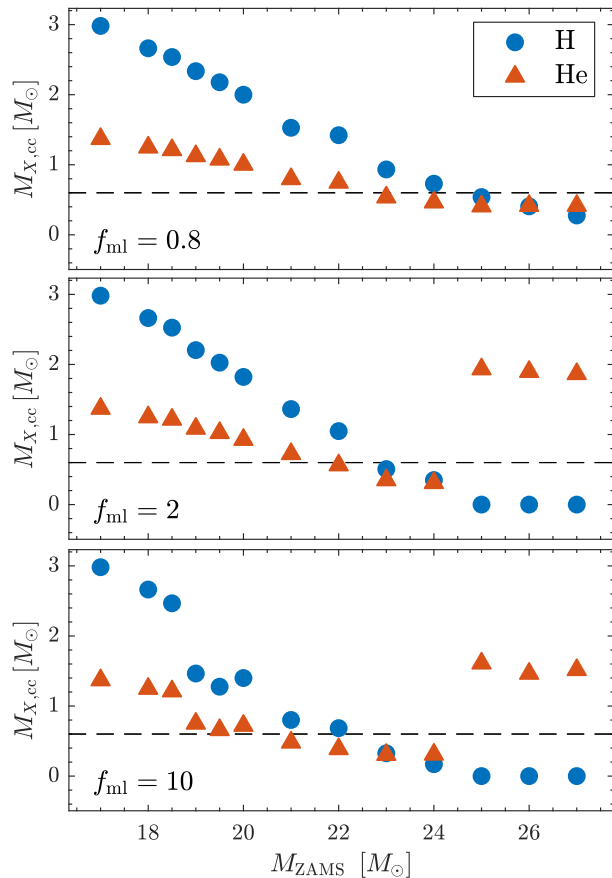


Figure 2. The final envelope mass of hydrogen (blue circles) and helium (orange triangles) as a function of the ZAMS mass. The three panels are for different mass-loss rate scaling factor, f_{ml} , inside the instability strip as the star crosses from right to left.

Moreover, models with $M_{\text{ZAMS}} \gtrsim 24M_{\odot}$ and enhanced mass-loss rate in the instability strip lose their entire hydrogen envelope, as we show for in Fig. 2, and become hot progenitors (WR stars) of SNe Ib. Other models lose most of their hydrogen envelope but still are left with $0.01M_{\odot} \lesssim M_{\text{H,cc}} \lesssim 0.5 - 1M_{\odot}$ of hydrogen in their envelope at core-collapse; these become the progenitors of SNe I Ib. We explain the different groups and their implications on the RSG problem with more detail in section 4.

Now we turn to examine the possibility of obscured CCSNe. We assume that the dense wind efficiently forms dust and calculate its optical depth. We consider the wind section from an inner radius of $R_{\text{in}} = 10^{16}$ cm (as the supernova will destroy dust at inner radii) and with a density of $\rho(r) = \dot{M}/4\pi v_w r^2$, where \dot{M} is the mass-loss rate and v_w is the wind velocity. We also take the opacity in the V-band to be $\kappa_V \approx 100 \text{ cm}^2 \text{ g}^{-1}$ (e.g.,

Kochanek et al. 2012), and derive

$$\begin{aligned} \tau_V &= \int_{R_{\text{in}}}^{R_{\text{out}}} \kappa_V \rho \, dr \\ &\simeq 5 \left(\frac{\dot{M}}{10^{-4} M_{\odot} \text{ yr}^{-1}} \right) \left(\frac{R_{\text{in}}}{10^{16} \text{ cm}} \right)^{-1} \\ &\quad \times \left(\frac{\kappa_V}{100 \text{ cm}^2 \text{ g}^{-1}} \right) \left(\frac{v_w}{10 \text{ km s}^{-1}} \right)^{-1}, \end{aligned} \quad (2)$$

where in the second equality we assume constant mass-loss rate and wind velocity and that $R_{\text{out}} \gg R_{\text{in}}$.

To derive a more accurate expression we take the mass-loss rate as function of time from our numerical results. The density, $\rho(r)$, at radius r corresponds to a mass-loss, $\dot{M}(t)$, at time $t = t_{\text{cc}} - r/v_w$, where t_{cc} is the time of core-collapse (explosion). We take v_w constant with time according to the following prescription. We simply assume that when the mass-loss rate in the strip is higher, the wind velocity is lower even after the star leaves the instability strip. For the default mass-loss rate, $f_{\text{ml}} = 0.8$, we take the wind velocity to be the escape velocity from the star at core-collapse, $v_{\text{esc,cc}}$. The wind velocity is then

$$v_w = v_{\text{esc,cc}} \left(\frac{f_{\text{ml}}}{0.8} \right)^{-1}. \quad (3)$$

Taking $r = v_w(t_{\text{cc}} - t)$ the expression for the optical depth is

$$\tau_V = \int_{t_{\text{out}}}^{t_{\text{in}}} \frac{\kappa_V \dot{M}(t)}{4\pi v_w^2 (t_{\text{cc}} - t)^2} dt. \quad (4)$$

We present the wind velocity according to equation (3) for the different models in the top row of Fig. 3. In the second row we present the average mass-loss rate in the last 100 years before explosion, and in the bottom row we present the optical depth according to equation (4) for $\kappa_V = 100 \text{ cm}^2/\text{g}$. We discuss the implications of the optical depth in section 4.

Another relevant quantity is the time after the model exists the instability strip and until explosion, which we present in Fig 4.

4. IMPLICATIONS TO THE RSG PROBLEM

Our introduction of the high mass-loss rate in the extension of the instability strip (following Yoon, & Cantiello 2010) splits the stars that enter the strip from right to left to four groups. (1) Stars that explodes while still suffering a very high mass-loss rate and are likely to be IR-bright but visibly faint. (2) Stars that leave the strip and explode as SNe II. (3) Stars that

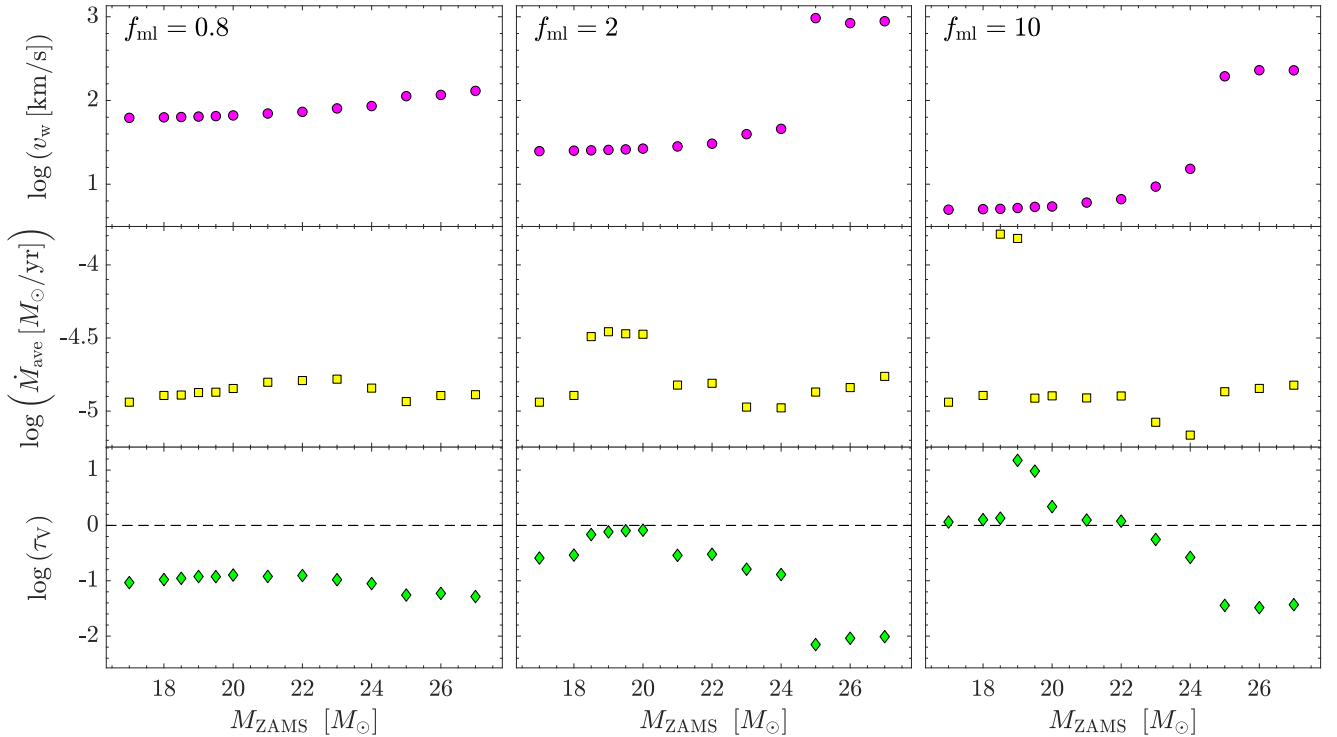


Figure 3. From top row to bottom and in logarithmic scales: The wind velocity according to equation (3), the average mass-loss rate in the last 100 yr before core-collapse, and the optical depth of the dust as given by equation (4) from an inner radius of $R_{\text{in}} = 10^{16}$ cm and opacity of $\kappa_V = 100 \text{ cm}^2 \text{ g}^{-1}$; the dashed black line marks: $\tau_V = 1$. We calculate each quantity for the 3 instability strip mass-loss scaling factors $f_{\text{ml}} = 0.8$ (left column), $f_{\text{ml}} = 2$ (middle column), and $f_{\text{ml}} = 10$ (right column).

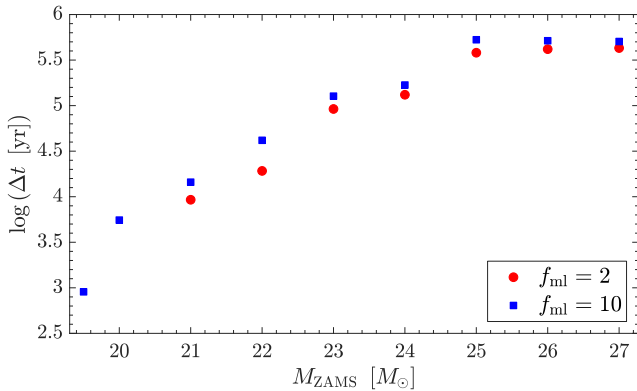


Figure 4. The time of explosion after exiting the instability strip as a function of ZAMS mass.

leave the strip and explode with hydrogen mass of $0.01M_{\odot} \lesssim M_{\text{H,cc}} \lesssim 0.5 - 1M_{\odot}$ and form SNe IIb. (4) Stars that lose all their hydrogen and explode as SNe Ib. We infer the mass range of each group from Figs. 2 and 3. Because of the large uncertainties in mass-loss rates, boundaries of the extension of the instability strip, and a possible influence by weak binary interaction (our scheme does not treat strong binary interaction), we take the boundaries between the groups as whole solar mass, beside one case.

4.1. Dust enshrouded IR bright CCSNe

From Fig. 3 we see that for $f_{\text{ml}} = 10$ in our mass-loss scheme this group comprises stars with initial masses of $M_{\text{S,IR}} \approx 18.5 - 20M_{\odot}$. We emphasise that the size of the instability strip in these high luminosities is uncertain, and the range might be somewhat larger. As well, our scheme refers only to single stars and those that suffer a weak binary interaction. Stars with a strong binary interaction require different calculations. We assume here and below that about half of the stars suffer only weak or no binary interaction. For an initial mass function (IMF) of $dN \propto M^{-2.35}dM$, we find this group to account for $F_{\text{S,IR}} \approx 2\%$ of all CCSNe. With weak binary interactions that enhance mass-loss and somewhat wider instability strip, this group might be $\approx 5\%$ of all CC-SNe. By a weak binary interaction, we refer to a weak to moderate spin-up by a companion or a weak tidal interaction. Our scheme does not include strong binary interactions where a companion determines the mass-loss rate, e.g., like a massive companion that enters a common envelope.

In discussing an explosion within a dust shell, we follow Kochanek et al. (2012) in treating obscuring by dust. They discuss several important processes, such as the presence of one type of dust, silicate (for massive

stars that we study here) or graphitic, and the emission by the dust shell. Since the dust shell is unresolved, its emission adds to the luminosity mainly in the IR. The observational finding of Jencson et al. (2019) show that there are IR-bright CCSNe that are (almost) undetectable in the visible, and so we need to consider obscuring in the visible. The optical depth in the visible of wind with constant velocity v_w and a constant mass-loss rate of \dot{M} is given by equation (2). In the lower row of Fig. 3 we present the optical depth in the V-band for a dusty wind that takes into account the mass-loss rate variation in our stellar evolution simulations (equation 4 from an inner radius $R_{\text{in}} = 10^{16}$ cm), but takes a constant wind velocity (equation 3).

Since the shell is not resolved, not all the photons in the visible that are scattered by dust are lost from our beam, and the decrease in the visible light is about a factor of few $\times 10$ for $\tau_V = 5$, or more than three magnitudes in the visible (Kochanek et al. 2012).

Shortly after the explosion the SN ejecta collides with the dense wind, the CSM. The interaction of the ejecta with the CSM converts kinetic energy to radiation. We scale the efficiency of this process to be $\epsilon_i = 0.1$ and the shock velocity into the CSM to be $v_s = 4000 \text{ km s}^{-1}$ (e.g., Fox et al. 2013, 2015)

$$L_i = \epsilon_i \dot{M} \frac{v_s^3}{2v_w} = 5.3 \times 10^6 \left(\frac{\dot{M}}{10^{-4} M_\odot \text{ yr}^{-1}} \right) \times \left(\frac{v_s}{4000 \text{ km s}^{-1}} \right)^3 \left(\frac{v_w}{10 \text{ km s}^{-1}} \right)^{-1} \left(\frac{\epsilon_i}{0.1} \right) L_\odot. \quad (5)$$

This corresponds to a bolometric magnitude of about -12 , fainter by several magnitudes relative to typical CCSNe. In addition, the dust that still resides at large distances will make the SN redder, and so the visual magnitude will be lower even relative to typical CCSNe. Such events might be classified at first place as intermediate luminosity optical transients (ILOTs), rather than CCSNe. But they are fainter in the visible and therefore will be detected in much lower numbers than CCSNe that are not enshrouded by a dense dusty wind.

We conclude that the dusty wind reduces the luminosity in the visible by several magnitudes. Present observations can still detect such type II CCSNe, but at much smaller numbers than their occurrence rate. As we write above, these are only for stars in the initial mass range of $M_{\text{S,IR}} \approx 18.5 - 20 M_\odot$.

4.2. Type II CCSNe

This group is of stars that have hydrogen mass at core-collapse of $M_{\text{H,cc}} \gtrsim 1 M_\odot$, and that are not enshrouded by optically thick dust. From Fig. 2 we find the upper mass of this group and from Fig. 3 its lower mass. These

give for the mass range of this group $M_{\text{S,II}} \simeq 20 - 21 M_\odot$. This mass range amounts to $\approx 2\%$ of all CCSNe, or $F_{\text{S,II}} \approx 1\%$ of all CCSNe if we take those that do not suffer strong binary interaction.

4.3. Type I Ib CCSNe

SNe I Ib are CCSNe that in the first several days have strong hydrogen lines, but later these lines substantially weaken and even disappear. This results from low hydrogen mass at explosion, about $M_{\text{H,cc}} \simeq 0.03 - 0.5 M_\odot$ (e.g., Meynet et al. 2015; Yoon et al. 2017), or even up to $M_{\text{H,env}} \leq 1 M_\odot$ (e.g., Sravan et al. 2018). SNe I Ib make $f_{\text{Ib,H}} \simeq 10 - 12\%$ of all CCSNe in high metallicity stellar populations (e.g., Sravan et al. 2018). From Fig. 2 we find that the relevant mass range for SNe I Ib progenitors in our $f_{\text{ml}} = 10$ case is $M_{\text{S,Ib}} \simeq 21 - 24 M_\odot$. For an IMF of $dN \propto M^{-2.35} dM$ this amounts to $\simeq 0.045$ of all CCSNe. However, if about half of these stars suffer strong binary interaction that our scheme does not consider, the single-star and weak binary interaction channels that we study here for SNe I Ib correspond to $F_{\text{S,Ib}} \approx 2\%$ of all CCSNe. We note that Naiman et al. (2019) crudely suggest that the single-star channel accounts for $\approx 2 - 4\%$ of all CCSNe (about $20 - 40\%$ of all SNe I Ib).

4.4. Type I b CCSNe

In the mass range we calculate here this group comes from stars with an initial mass of $M_{\text{S,Ib}} \gtrsim 24$, as we see from Fig. 2. This range amounts to $\simeq 20\%$ of all CCSNe if we take the upper mass limit to be $M_{\text{ZAMS}} = 100 M_\odot$. If we consider that about half suffer strong binary interaction, the single star evolution (including weak binary interactions) that we study here amounts to $F_{\text{S,Ib}} \approx 10\%$ of all CCSNe. Some of them might lose also all their helium and lead to SNe Ic.

Our finding that most, $\simeq 2/3$, of the stars with $M_{\text{S,Ib}} \gtrsim 18$ form SNe Ib and possibly SNe Ic, is compatible with the finding of Smartt (2015).

5. SUMMARY

We are motivated by the theoretical disagreement on the fate of star with ZAMS mass of $M_{\text{ZAMS}} \gtrsim 18 M_\odot$ (section 1), and by the new observations of IR-bright but visibly faint CCSNe (Jencson et al. 2019). Using the numerical stellar evolution code MESA we have simulated the evolution of 48 stellar models to the point of core-collapse and explored the effect of an enhanced mass-loss inside the instability strip as the evolved stars cross from right to left at very high luminosities. Based on Yoon, & Cantiello (2010) we assumed an enhanced mass-loss rate as the star crosses the instability strip

from right to left at high luminosities (grey area of the instability strip on Fig. 1). Our mass-loss prescription is for single star evolution and possibly weak binary interaction. We do not include strong binary interaction.

We concentrated on two pre-core-collapse stellar properties, the stellar hydrogen mass (Fig. 2), and the optical depth of the dusty wind (Fig. 3). From these properties we divide the stars that enter or cross the upper (extension) instability strip to four groups with very uncertain mass boundaries between them. (1) Stars that explode as SNe II while they are in the strip and therefore are enshrouded by dust (section 4.1). These have initial mass in the range of $M_{S,IR} \simeq 18.5 - 20M_{\odot}$. (2) Stars that leave the instability strip from the left and explode as SNe II. They have $M_{S,II} \simeq 20 - 21M_{\odot}$ (section 4.2). (3) Stars that leave the strip and at core-collapse have a hydrogen mass of $M_{H,cc} \lesssim 0.5 - 1M_{\odot}$. They explode as SNe IIb and have $M_{S,IIb} \simeq 21 - 24M_{\odot}$ (section 4.3). (4) Stars that leave the strip and explode as SNe Ib and possibly as SNe Ic. These have $M_{S,Ib} \gtrsim 24$ (section 4.4).

Because the mass boundaries of the four groups are highly uncertain, so are the fraction F_S of each group is highly uncertain. Our estimated fractions of CCSNe in each of these four groups are $F_{S,IR} \approx 2\%$, $F_{S,II} \approx 1\%$, $F_{S,IIb} \approx 2\%$, and $F_{S,Ib} \approx 10\%$, respectively. In estimating these fractions we used the IMF of $dN \propto M^{-2.35}dM$ with a maximum mass of $100M_{\odot}$ and assumed that about half of the stars suffer strong binary interaction that we do not consider here. Therefore, our assumption of enhanced mass-loss while in the instability strip

implies that single star evolution brings only a fraction of

$$\eta_{S,II} \equiv \frac{F_{S,II} + F_{S,IIb}}{F_{S,IR} + F_{S,II} + F_{S,IIb} + F_{S,Ib}} \approx 20\% \quad (6)$$

of stars with $M_{ZAMS} \gtrsim 18.5M_{\odot}$ to end as SNe II or SNe IIb that are not heavily enshrouded by dusty CSM.

Smartt (2015) lists 30 progenitors of SN type II or IIb which all have a ZAMS mass of $M_{ZAMS} \lesssim 18M_{\odot}$. From that he argues that the IMF implies that if all these stars explode there should be ≈ 13 CCSNe of types II and IIb with a progenitor of $M_{ZAMS} \gtrsim 18M_{\odot}$. According to our analysis (equation 6) we expect that out of these 13 SNe with progenitor mass $M_{ZAMS} \gtrsim 18M_{\odot}$, only $\approx 2 - 3$ are SNe II or IIb (and binary interaction can reduce this number further by forming more SNe Ibc)¹.

Our main conclusion is that the statistical uncertainties are too large to decide whether many stars with $M_{ZAMS} \gtrsim 18M_{\odot}$ do not explode as expected in the neutrino driven explosion mechanism, or whether most of them form SNe Ibc and obscured SNe II that are IR-bright, as expected by the jittering jets explosion mechanism.

ACKNOWLEDGEMENTS

This research was supported by a grant from the Israel Science Foundation. N.S. research is partially supported by the Charles Wolfson Academic Chair.

REFERENCES

- Adams, S. M., Kochanek, C. S., Gerke, J. R., Stanek K. Z., Dai X., 2017, MNRAS, 468, 4968
- Bethe, H. A., & Wilson, J. R. 1985, ApJ, 295, 14
- Blondin, J. M., & Mezzacappa, A. 2007, Nature, 445, 58
- Brott, I., de Mink, S. E., Cantiello, M., et al. 2011, Astronomy and Astrophysics, 530, A115
- Couch, S. M., & Ott, C. D. 2013, ApJL, 778, L7
- Couch, S. M., & Ott, C. D. 2015, ApJ, 799, 5
- de Jager, C., Nieuwenhuijzen, H., van der Hucht, K. A. 1988, A&AS, 72, 259
- Ertl T., Janka, H.-T., Woosley S. E., Sukhbold, T., Ugliano M., 2016, ApJ, 818, 124
- Ertl T., Woosley S. E., Sukhbold, T., Janka, H.-T., 2019, arXiv:1910.01641
- Fernández, R. 2015, MNRAS, 452, 2071
- Fox O. D., Filippenko A. V., Skrutskie M. F., Silverman J. M., Ganeshalingam M., Cenko S. B., Clubb K. I., 2013, AJ, 146, 2
- Fox, O. D., Smith, N., Ammons, S. M., et al. 2015, MNRAS, 454, 4366
- Fryer, C. L. 1999, ApJ, 522, 413
- Gerke, J. R., Kochanek, C. S., & Stanek, K. Z. 2015, MNRAS, 450, 3289
- Georgy, C., Ekström, S., Eggenberger, P., et al. 2013, A&A, 558, A103
- Gilkis, A., & Soker, N. 2014, MNRAS, 439, 4011
- Gilkis, A., & Soker, N. 2015, ApJ, 806, 28

¹ At the Symposium "The Deaths and Afterlives of Stars" (Space Telescope Science Institute, April 22-24, 2019) Smartt updated the observed number of progenitors with $M_{ZAMS} \lesssim 18M_{\odot}$ to 35 (<https://cloudproject.hosted.panopto.com/Panopto/Pages/Viewer.aspx?id=468178583b9c-4825-8005-aa3700f5dfb0>). In this case 15 progenitors with a mass of $M_{ZAMS} \gtrsim 18M_{\odot}$ are expected. By our analysis, only 3 of them should be type II or IIb CCSNe.

- Gilkis, A., Soker, N., & Papish, O. 2016, *ApJ*, 826, 178
- Glebbeeck, E., Gaburov, E., de Mink, S. E., et al. 2009, *A&A*, 497, 255
- Heger, A., Jeannin, L., Langer, N., et al. 1997, *A&A*, 327, 224
- Henyey, L., Vardya, M. S., & Bodenheimer, P. 1965, *The Astrophysical Journal*, 142, 841
- Horiuchi, S., Nakamura, K., Takiwaki, T., Kotake K., Tanaka M., 2014, *MNRAS*, 445, L99
- Iwakami, W., Nagakura, H., & Yamada, S. 2014, *ApJ*, 793, 5
- Jencson, J. E., Kasliwal, M. M., Johansson, J., et al. 2017, *ApJ*, 837, 167
- Jencson, J. E., Kasliwal, M. M., Adams, S. M., et al. 2019, arXiv e-prints, arXiv:1901.00871
- Jennings, Z. G., Williams, B. F., Murphy, J. W., Dalcanton, J. J., Gilbert, K. M., Dolphin, A. E., Weisz, D. R., Fouesneau, M. 2014, *ApJ*, 795, 170
- Kashi, A., & Soker, N. 2017, *MNRAS*, 467, 3299
- Kazeroni, R., Guilet, J., & Foglizzo, T. 2017, arXiv:1701.07029
- Kuroda T., Takiwaki T., & Kotake K., 2014, *Phys. Rev. D*, 89, 044011
- Kochanek, C. S., Khan, R., & Dai, X. 2012, *ApJ*, 759, 20
- Kushnir, D. 2015, arXiv:1506.02655
- Langer, N., Fricke, K. J., & Sugimoto, D. 1983, *Astronomy and Astrophysics*, 126, 207
- Lovegrove, E., & Woosley, S. E. 2013, *ApJ*, 769, 109
- Maeder, A., & Meynet, G. 2001, *Astronomy and Astrophysics*, 373, 555
- Meynet, G., Chomienne, V., Ekström, S., et al. 2015, *A&A*, 575, A60
- Mueller, B., & Janka, H.-T. 2015, *MNRAS*, 448, 2141
- Müller, B., Melson, T., Heger, A., & Janka, H.-T. 2017, *MNRAS*, 472, 491
- Müller, B., Tauris, T. M., Heger, A., et al. 2019, *MNRAS*, 484, 3307
- Nadezhin, D. K. 1980, *Ap&SS*, 69, 115
- Naiman B., Sabach E., Gilkis A., Soker N., 2019, arXiv, arXiv:1909.04583
- Nugis, T., & Lamers, H. J. G. L. M. 2000, *A&A*, 360, 227
- Papish, O., Nordhaus, J., & Soker, N. 2015, *MNRAS*, 448, 2362
- Paxton, B., Bildsten, L., Dotter, A., Herwig, F., Lesaffre, P., & Timmes, F. 2011, *ApJS*, 192, 3
- Paxton, B., Cantiello, M., Arras, P., et al. 2013, *ApJS*, 208, 4
- Paxton, B., Marchant, P., Schwab, J., et al. 2015, *ApJS*, 220, 15
- Paxton, B., Schwab, J., Bauer, E. B., et al. 2018, *The Astrophysical Journal Supplement Series*, 234, 34
- Quataert, E., Lecoanet, D., & Coughlin, E. R. 2019, *MNRAS*, 485, L83
- Smartt, S. J. 2015, *PASA*, 32, e016
- Smartt, S. J., Eldridge, J. J., Crockett, R. M., Maund, J. R. 2009, *MNRAS*, 395, 1409
- Smith, N., Li, W., Miller, A. A., et al. 2011, *ApJ*, 732, 63
- Soker, N. 2010, *MNRAS*, 401, 2793
- Soker, N. 2016, *NewAR*, 75, 1
- Soker, N. 2018, arXiv:1805.03447
- Soker, N. 2019a, *Research in Astronomy and Astrophysics*, in press (arXiv:1810.09074)
- Soker, N. 2019b, arXiv e-prints, arXiv:1907.13312
- Pravdan, N., Marchant, P., & Kalogera, V. 2018, arXiv:1808.07580
- Sukhbold, T., & Adams, S. 2019, arXiv e-prints, arXiv:1905.00474
- Sukhbold T., Ertl, T., Woosley, S. E., Brown, J. M., Janka, H.-T., 2016, *ApJ*, 821, 38
- Van Dyk, S. D., Zheng, W., Brink, T. G., et al. 2018, *ApJ*, 860, 90
- Vink, J. S., de Koter, A., & Lamers, H. J. G. L. M. 2001, *A&A*, 369, 574
- Walmswell, J. J., & Eldridge, J. J. 2012, *MNRAS*, 419, 2054
- Williams B. F., Peterson, S., Murphy, J., Gilbert, K., Dalcanton, J. J., Dolphin, A. E., Jennings, Z. G., 2014, *ApJ*, 791, 105
- Yoon, S.-C., & Cantiello, M. 2010, *ApJL*, 717, L62
- Yoon, S.-C., Dessart, L., & Clocchiatti, A. 2017, *ApJ*, 840, 10